The Astrophysical Journal Supplement Series, 239:19 (13pp), 2018 December https://doi.org/10.3847/1538-4365/aae924

WINERED High-resolution Near-infrared Line Catalog: A-type Star

Hiroaki Sameshima[1], Yuji Ikeda[1,2], Noriyuki Matsunaga[1,3], Kei Fukue[1], Naoto Kobayashi[1,4,5], Sohei Kondo[1], Satoshi Hamano[1], Hideyo Kawakita[1,6], Chikako Yasui[1,7], Natsuko Izumi[7], Misaki Mizumoto[8], Shogo Otsubo[1,6], Keiichi Takenaka[1,6], Ayaka Watase[1,6], Akira Asano[1,6], and Tomohiro Yoshikawa[9]

[1] Laboratory of Infrared High-resolution spectroscopy (LiH), Koyama Astronomical Observatory, Kyoto Sangyo University, Motoyama, Kamigamo, Kita-ku, Kyoto 603-8555, Japan; sameshima@cc.kyoto-su.ac.jp
[2] Photocoding, 460-102 Iwakura-Nakamachi, Sakyo-ku, Kyoto,606-0025, Japan
[3] Department of Astronomy, Graduate School of Science, The University of Tokyo, 7-3-1 Hongo, Bunkyo-ku, Tokyo 113-0033, Japan
[4] Kiso Observatory, Institute of Astronomy, School of Science, The University of Tokyo, 10762-30 Mitake, Kiso machi, Kiso-gun, Nagano, 397-0101, Japan
[5] Institute of Astronomy, School of Science, The University of Tokyo, 2-21-1 Osawa, Mitaka, Tokyo 181-0015, Japan
[6] Department of Physics, Faculty of Sciences, Kyoto Sangyo University, Motoyama, Kamigamo, Kita-ku, Kyoto 603-8555, Japan
[7] National Astronomical Observatory of Japan, 2-21-1 Osawa, Mitaka, Tokyo 181-8588, Japan
[8] Centre for Extragalactic Astronomy, Department of Physics, University of Durham, South Road, Durham DH1 3LE, UK
[9] Edechs, 17-203 Iwakura-Minami-Osagi-cho, Sakyo-ku, Kyoto 606-0003, Japan
Received 2018 August 12; revised 2018 October 15; accepted 2018 October 15; published 2018 November 26

Abstract

We present a catalog of absorption lines in the z', Y, and J bands that we identified in 21 Lyn, a slowly rotating A0.5 V star. We detected 155 absorption features in the high-resolution (0.90–1.35 μm, $R = 28{,}000$) spectrum obtained with the WINERED spectrograph after the telluric absorption was carefully removed using a spectrum of a B-type star as a telluric standard. With a visual comparison with synthetic spectra, we compiled a catalog of 219 atomic lines for the 155 features, some of which are composed of multiple fine structure lines. The high-quality WINERED spectrum enabled us to detect a large number of weak lines down to ∼1% in depth, which are identified for an A-type star for the first time. The catalog includes the lines of H, C, N, O, Mg, Al, Si, S, Ca, Fe, and Sr. These new lines are expected to be useful for spectral classification and chemical abundance analyses, while the line catalog is useful for observers who plan to use A-type stars as telluric standards because it is necessary to distinguish between stellar lines and telluric absorption lines in high-resolution spectra. ASCII versions of the spectra are available in the online version of the journal.

Key words: atlases – line: identification – stars: fundamental parameters – stars: individual (21 Lyn)

Supporting material: data behind figure, extended figure, machine-readable tables

1. Introduction

Recent progress in near-infrared (NIR) spectrographs has enabled us to obtain NIR high-resolution and high-quality spectra of stars and made it possible to derive fundamental parameters including chemical abundances. However, reliable line catalogs in the NIR region have yet to be established. One of the most reliable NIR line catalogs based on astronomical observation was given by Meléndez & Barbuy (1999); they built a line catalog in the wavelength ranges of 1.00–1.34 and 1.49–1.80 μm using the solar spectrum obtained with a Fourier transform spectrometer (Livingston & Wallace 1991). However, because their line catalog is based on the solar spectrum, it does not cover lines that do not appear in the solar spectrum and hence is applicable only to stars with limited spectral types.

Aiming to extend the coverage of line catalogs in both the wavelength and spectral type directions, we are carrying out a project to establish NIR line catalogs based on observations of various types of stars using our high-dispersion echelle spectrograph, WINERED (Ikeda et al. 2016). In the WIDE mode, WINERED covers the wavelength range of 0.90–1.35 μm (corresponding to the z', Y, and J bands) with a resolving power of $R \equiv \lambda/\Delta\lambda = 28{,}000$. The high throughput of WINERED enables us to obtain high-quality spectra—the typical signal-to-noise ratio being $\gtrsim$300 for luminous stars—with short-time exposures.

As the first step of our project, we present a line catalog produced from the spectra of an A-type star obtained with WINERED. Surprisingly, very little spectroscopic studies have been carried out for A-type stars in the wavelength range of 0.90–1.35 μm. The most reliable spectral atlas of A-type stars in this range was previously given by Wallace et al. (2000), who presented J-band spectra for 88 fundamental MK standard stars. However, because the resolving power was limited to $R \sim 3000$, their spectra of A-type stars such as HR 4534 (A3 V) show a very limited number of lines besides hydrogen lines. High-resolution spectroscopic observation is thus necessary to investigate the weak absorption lines in A-type stars. On the other hand, given that the spectral lines in A-type stars are rotationally broadened in general, the resolution of WINERED is sufficient to resolve each line.

The line catalog of an A-type star is useful not only for scientific studies of A-type stars but also for making use of A-type stars as telluric standards. In low-resolution spectroscopic observations, A-type stars have been widely used as telluric standard stars owing to their relatively featureless spectra (except for strong hydrogen lines). However, their weak metal lines get resolved when the spectral resolution is high (e.g., $R > 10{,}000$), which complicates the telluric correction unless the intrinsic stellar lines are carefully removed (Sameshima et al. 2018). The line catalog in the present work would help to distinguish between stellar lines and telluric absorption lines in the spectra of A-type stars.

Throughout this paper, we use air wavelengths rather than vacuum wavelengths unless otherwise noted.

Table 1
Observation Log

Parameter	21 Lyn	HD 43384
Spectral type	A0.5 V	B3 Iab
Obs. Time (UT)	2014 Jan 23 15:00	2014 Jan 23 14:26
Airmass	1.04–1.06	1.07–1.10
Exposure	200 s × 6	360 s × 4
Dithering	ABBAAB	ABBA
Signal-to-noise ratio	830	580

Note. The spectral types are retrieved from the SIMBAD astronomical database. The signal-to-noise ratio is measured from the standard deviation of the continuum level of the coadded spectrum at $\sim$1.04 μm, where telluric absorption is almost negligible.

2. Data Acquisition and Reduction

A slowly rotating star is desirable as our target to produce the line catalog because the absorption lines are relatively deep and less affected by line blending and the identification task becomes easier. However, slowly rotating A-type stars often show chemical peculiarities (e.g., Preston 1974; Abt & Morrell 1995). Royer et al. (2014) performed a cluster analysis of 47 A0–A1 stars with low projected rotational velocity (hereafter, $v \sin i$) and split them into chemically peculiar (CP) and normal stars. Among the normal stars that they identified, 21 Lyn (A0.5 V, $v \sin i = 19$ km s^{-1}) was observed with WINERED, giving a high-quality spectrum that can be used for our purpose.

The observation of 21 Lyn was carried out on 2014 January 23 using the WINERED echelle spectrograph mounted on the 1.3 m Araki Telescope at the Koyama Astronomical Observatory in Kyoto, Japan. The observation mode was set to the WIDE mode with the 100 μm width slit, which realizes a coverage of 0.90–1.35 μm and a resolving power of $R = 28{,}000$. The target was observed at two positions separated by about 30$''$ along the slit by nodding the telescope to make the ABBA dithering sequence. The observation log is summarized in Table 1.

All data were reduced in a standard manner using IRAF[10] routines as follows. Sky subtraction was performed by taking the difference between two consecutive images taken at different slit positions, i.e., A−B and B−A. Scattered light was evaluated at the interorder regions of each difference image and then removed. Flat-fielding was performed using a dome-flat image. Bad pixels were then masked and replaced by linear interpolation from the surrounding pixels. Owing to the large value of the γ angle of WINERED, the spectral lines in the two-dimensional images were tilted with respect to the dispersion direction; this tilt was corrected by performing a geometrical transformation using arc-lamp images as a reference. Then, one-dimensional spectra were extracted using the IRAF task `apall`. Wavelength calibration was performed using Th–Ar lamp spectra that were extracted in the same way as the target object. Normalization of each frame was performed by the IRAF task `continuum`, where cubic spline curves or low-order Legendre polynomials were mainly used to fit the continuum. These frames were then coadded by averaging the counts for each pixel, in which spurious features were carefully checked by eye and masked.

The B-type star HD 43384 (B3 Iab), which was observed just before 21 Lyn with almost the same airmass (see Table 1), was used as a telluric calibration source. From the continuum-normalized spectrum of HD 43384 reduced in the same way as 21 Lyn, intrinsic stellar lines were carefully distinguished from telluric absorption lines by using synthetic telluric spectra created by `molecfit` (Kausch et al. 2015; Smette et al. 2015) as a reference. These stellar lines and features other than telluric absorption were removed by fitting multiple Gaussian curves (see Sameshima et al. 2018 for the details). The telluric spectra retrieved in this way were used to remove the telluric absorption from the 21 Lyn spectra by the IRAF task `telluric`, where the difference in the effective airmass was corrected following Beer's law (Beer 1852). Finally, we obtained the telluric corrected spectrum of 21 Lyn for the wavelength ranges of 0.910–0.930, 0.960–1.115, and 1.160–1.330 μm, which correspond to the z', Y, and J bands, respectively. Note that we could not obtain the appropriate spectra for the wavelength range of 1.307–1.312 μm owing to the nonlinear response of the bad pixel region on the array; we decided not to use this part of the spectra in the following analysis.

After telluric correction, continuum normalization was again performed by the IRAF task `continuum` to improve the normalization. This was especially important around the wavelength ranges where the first normalization performed before telluric correction was complicated by telluric absorption lines. Note that we could not perform normalization around the hydrogen lines in the straightforward manner described above because these lines were often not fully covered within a single order owing to their large width. We therefore determined the continuum levels around the hydrogen lines so that their line profiles match synthetic spectra, which prevents quantitative discussions about the hydrogen lines. The continuum-normalized spectra of 21 Lyn are shown in Figure 1, where the wavelengths are not heliocentric but corrected to be at rest in air by cross-correlation matching with synthetic spectra. In the figure, the telluric spectra created above are also wavelength-shifted by the same amount of 21 Lyn and shown in the lower panels. The symbol $\oplus$ indicates the spectral regions where we concluded that spurious features remain even after the telluric correction. ASCII versions of the 21 Lyn and the telluric spectra are available in the online version of the journal.

3. Line Identification

To identify lines in the observed spectrum, we first created model spectra of 21 Lyn with ATLAS9 (Kurucz 1993). Fundamental stellar parameters were adopted from Royer et al. (2014), who derived the following parameters of 21 Lyn from an optical high-resolution spectrum: the effective temperature, the surface gravity, the microturbulence, $v \sin i$, and the chemical abundances (C, O, Mg, Si, Ca, Sc, Ti, Cr, Fe, Ni, Sr, Y, Zr, and Ba). The other elemental abundances were set to the solar values, and the solar abundance was taken from Grevesse & Sauval (1998). The adopted parameters are summarized in Table 2. The excitation potentials, transition terms, oscillator strengths ($\log gf$), and damping constants of the spectral lines used for spectral synthesis were retrieved from the Vienna Atomic Line Database (VALD;

[10] IRAF is distributed by the National Optical Astronomy Observatories, which are operated by the Association of Universities for Research in Astronomy, Inc., under cooperative agreement with the National Science Foundation.

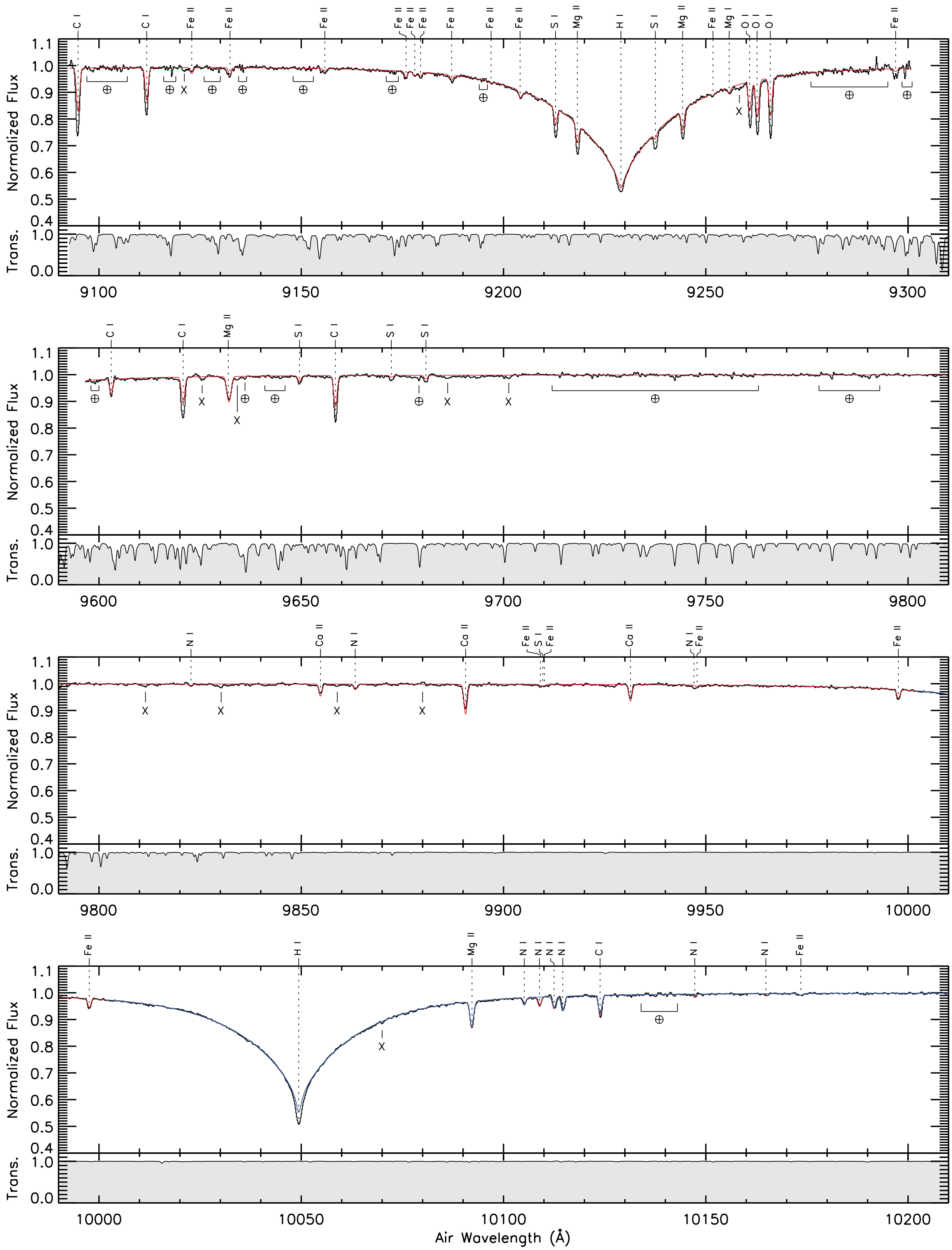

Figure 1. For each wavelength range, two panels present the spectra of 21 Lyn (upper) and the atmospheric transmittance (lower). Upper panel: continuum-normalized spectrum of 21 Lyn. The synthetic spectra created by ATLAS9 based on the oscillator strengths of the VALD database and those of Meléndez & Barbuy (1999) are indicated by red and blue lines, respectively. The symbol "X" indicates potentially significant features that are not identified in the VALD or MB99 in our analysis, while the symbol ⊕ indicates the spectral regions that show spurious features caused by imperfect correction of telluric absorption lines. Lower panel: atmospheric transmittance derived from the spectrum of the telluric standard star. The data used to create this figure are available. (An extended version of this figure is available.)

Table 2
Parameters of the Synthetic Spectra for 21 Lyn

Parameter	Value
Effective temperature: $T_{\rm eff}$ (K)	9520 ± 125
Surface gravity: $\log g$	3.79 ± 0.2
Microturbulence: ξ (km s^{-1})	1.7 ± 0.5
Rotational velocity: $v \sin i$ (km s^{-1})	18.7 ± 0.4
Elemental abundance	
Carbon: [C/H] with $\log \varepsilon_{\rm C,\odot} = 8.52$	−0.452 ± 0.056
Oxygen: [O/H] with $\log \varepsilon_{\rm O,\odot} = 8.83$	−0.246 ± 0.056
Magnesium: [Mg/H] with $\log \varepsilon_{\rm Mg,\odot} = 7.58$	−0.065 ± 0.175
Silicon: [Si/H] with $\log \varepsilon_{\rm Si,\odot} = 7.55$	+0.269 ± 0.221
Calcium: [Ca/H] with $\log \varepsilon_{\rm Ca,\odot} = 6.36$	−0.057 ± 0.417
Scandium: [Sc/H] with $\log \varepsilon_{\rm Sc,\odot} = 3.17$	−0.466 ± 0.118
Titanium: [Ti/H] with $\log \varepsilon_{\rm Ti,\odot} = 5.02$	−0.165 ± 0.085
Chromium: [Cr/H] with $\log \varepsilon_{\rm Cr,\odot} = 5.67$	+0.055 ± 0.078
Iron: [Fe/H] with $\log \varepsilon_{\rm Fe,\odot} = 7.50$	−0.004 ± 0.124
Nickel: [Ni/H] with $\log \varepsilon_{\rm Ni,\odot} = 6.25$	+0.287 ± 0.136
Strontium: [Sr/H] with $\log \varepsilon_{\rm Sr,\odot} = 2.97$	+0.410 ± 0.150
Yttrium: [Y/H] with $\log \varepsilon_{\rm Y,\odot} = 2.24$	+0.313 ± 0.105
Zirconium: [Zr/H] with $\log \varepsilon_{\rm Zr,\odot} = 2.60$	+0.550 ± 0.097
Barium: [Ba/H] with $\log \varepsilon_{\rm Ba,\odot} = 2.13$	+0.912 ± 0.168

Note. The solar abundance for each element, indicated in the left column, was adopted from Grevesse & Sauval (1998) in both this study and Royer et al. (2014), who obtained the parameters in this table.

Piskunov et al. 1995; Kupka et al. 1999; Ryabchikova et al. 2015), which is a compilation of literature information of lines based mainly on theoretical calculations. In addition, the solar-based line catalog given by Meléndez & Barbuy (1999; hereafter MB99) was also used for spectral synthesis. Note that their line catalog covers 10,000 Å and longer; therefore, the synthetic spectrum created with it does not cover the wavelength range shorter than 1.0 μm.

From visual inspection of the observed and synthetic spectra, we detected 155 absorption features including very wide hydrogen lines (Pa β, Pa γ, Pa δ, and Pa ζ). Each absorption feature detected was fitted with a single Gaussian curve to measure the line depth, the FWHM, and the equivalent width. The depth was measured in percentage from the continuum level, 0% (with no visible absorption) to 100% (the maximum depth). When the absorption feature could not be reproduced with a single Gaussian curve, we measured the equivalent width by fitting multiple Gaussian curves and defined the depth of the deepest pixel as the line depth, while the FWHM was not obtained. Hydrogen lines were not measured because their spectral information was destroyed at the normalization step, as described above. The results of the measurements for the absorption features are summarized in Table 3.

The absorption features were classified according to the strengths in the following manner. The upper panel of Figure 2 shows a histogram of the measured depths for the absorption features fitted by single Gaussians. The number of lines increases toward weak lines, peaks at around 2%, and then decreases, indicating that the completeness of line detection changes at a depth around 2%. The lower panel of Figure 2 compares the measured FWHM with the depth of the same lines. The scatter in the measured FWHM increases with decreasing depth, which is simply due to the random noise of

Table 3
Measurement of the Absorption Features in 21 Lyn

ID	$\lambda_{\rm air}$ (Å)	Depth (%)	EW (mÅ)	FWHM (km s^{-1})	Rank	Elements
1	9094.8	26.7	277.9	32.1	1	C I
2	9111.8	18.6	181.8	29.9	1	C I
3	9122.9	1.6	14.4	27.2	3	Fe II
4	9132.4	3.4	46.5	42.4	2	Fe II
5	9155.8	1.9	30.2	48.2	3	Fe II
6	9175.7	2.8	30.3	31.1	2	Fe II
7	9178.1	1.5	18.9	36.7	3	Fe II
8	9179.5	2.3	20.8	27.0	2	Fe II
9	9187.2	2.5	34.1	41.0	2	Fe II
10	9196.9	0.9	5.9	19.8	3	Fe II
11	9204.1	2.7	33.1	34.5	2F	Fe II
12	9212.9	11.6	128.8	28.5	1	S I
13	9218.3	11.9	144.6	29.1	1	Mg II
14	9229.0	…	…	…	1	H I (Pa ζ)
15	9237.5	6.1	80.0	29.8	1	S I
16	9244.3	11.4	138.7	31.3	1	Mg II
17	9251.8	1.2	8.9	20.7	3	Fe II
18	9255.8	2.2	29.3	36.7	2	Mg I
19	9260.8	17.5	168.6	27.7	1F	O I
20	9262.8	20.6	211.8	29.4	1F	O I
21	9266.0	23.0	224.2	28.1	1F	O I
22	9296.9	5.7	56.8	30.1	1	Fe II
23	9603.0	7.6	62.9	24.0	1	C I
24	9620.8	15.9	176.6	32.1	1	C I
25	9631.9	8.3	109.2	37.9	1F	Mg II
26	9649.6	3.0	29.4	28.8	2	S I
27	9658.4	17.8	169.4	27.6	1	C I
28	9672.3	1.7	21.7	…	3F	S I
29	9680.8	2.7	30.0	32.7	2F	S I
30	9822.8	1.1	13.0	34.3	3	N I
31	9854.8	3.8	35.5	27.0	2	Ca II
32	9863.3	1.7	18.7	31.6	3	N I
33	9890.6	8.8	86.4	28.0	1F	Ca II
34	9909.7	1.3	29.2	…	3B	Fe II, S I
35	9931.4	5.6	53.0	27.1	1	Ca II
36	9947.1	0.8	10.0	…	3B	N I, Fe II
37	9997.6	3.9	38.2	26.7	2	Fe II
38	10049.4	…	…	…	1	H I (Pa δ)
39	10092.1	10.0	115.0	31.1	1F	Mg II
40	10105.1	2.4	19.8	22.5	2	N I
41	10108.9	3.4	31.2	25.3	2	N I
42	10112.5	4.9	48.2	27.1	2	N I
43	10114.6	5.1	49.4	26.9	1	N I
44	10123.9	8.6	90.2	28.9	1	C I
45	10147.3	1.4	9.1	18.6	3	N I
46	10164.8	0.9	9.7	29.1	3	N I
47	10173.5	0.8	15.4	50.9	3	Fe II
48	10216.3	1.0	11.8	33.6	3	Fe I
49	10245.6	0.6	8.8	41.6	3	Fe II
50	10327.3	5.0	50.9	28.0	2	Sr II
51	10332.9	0.9	12.5	37.8	3	Fe II
52	10366.2	1.0	11.9	31.9	3	Fe II
53	10371.3	0.8	9.1	30.8	3	Si I
54	10452.8	1.0	7.1	18.7	3	C I
55	10455.5	12.0	122.9	27.5	1	S I
56	10456.8	4.2	44.4	28.7	2	S I
57	10459.5	9.6	100.0	28.1	1	S I
58	10463.0	0.7	5.9	22.1	3	Fe II
59	10471.0	0.7	8.0	31.6	3	C I
60	10501.5	2.2	28.3	34.7	2	Fe II
61	10507.0	1.6	13.3	21.8	3	N I
62	10513.4	1.0	10.8	27.8	3	N I
63	10520.6	1.7	27.8	42.8	3	N I

Table 3
(Continued)

ID	λ_{air} (Å)	Depth (%)	EW (mÅ)	FWHM (km s^{-1})	Rank	Elements
64	10525.2	0.9	10.3	30.9	3	Fe II
65	10539.6	3.7	37.7	27.1	2	N I
66	10541.2	0.9	10.2	28.9	3	C I
67	10546.3	1.0	15.7	40.8	3	Fe II
68	10549.6	1.8	14.8	21.4	3	N I
69	10585.1	3.8	39.2	27.8	2	Si I
70	10603.4	2.0	19.3	25.3	2	Si I
71	10636.0	3.5	37.7	28.4	2	S I
72	10644.0	0.5	4.8	25.2	3	N I
73	10653.0	1.4	20.6	38.7	3	N I
74	10661.0	2.4	26.1	28.4	2	Si I
75	10675.7	2.0	34.4	46.5	3F	O I
76	10683.1	22.6	239.4	27.8	1	C I
77	10685.3	18.3	192.7	27.6	1	C I
78	10691.2	25.1	264.1	27.6	1	C I
79	10694.3	2.1	22.4	28.2	2	Si I
80	10707.3	15.8	166.3	27.5	1	C I
81	10713.5	0.8	11.9	38.7	3	N I
82	10727.4	2.3	25.7	29.2	2	Si I
83	10729.5	14.6	157.2	28.1	1	C I
84	10749.4	2.1	20.8	26.0	2	Si I
85	10754.0	2.9	33.0	29.6	2	C I
86	10757.9	0.4	2.7	18.7	3	N I
87	10786.8	1.6	17.2	27.6	3	Si I
88	10811.1	3.7	48.7	34.0	2F	Mg I
89	10827.1	5.6	60.1	27.9	1	Si I
90	10843.9	1.2	7.1	16.0	3	Si I
91	10862.7	2.7	36.9	35.7	2	Fe II
92	10868.8	0.8	3.0	9.2	3	Si I
93	10869.5	2.2	16.3	19.3	2	Si I
94	10885.3	0.9	15.0	42.7	3	Si I
95	10914.2	11.9	192.3	⋯	1B	Mg II, Sr II
96	10938.1	⋯	⋯	⋯	1	H I (Pa γ)
97	10951.8	5.9	73.7	27.2	1	Mg II
98	10965.5	1.0	11.7	27.7	3	Mg I
99	10979.3	1.0	12.8	31.1	3	Si I
100	10982.1	0.7	7.0	23.5	3	Si I
101	11018.0	2.2	24.1	28.0	2	Si I
102	11125.6	1.6	21.9	34.6	3	Fe II
103	11601.8	1.3	22.0	37.8	3	S I
104	11619.3	4.4	39.1	21.5	2	C I
105	11628.8	6.1	72.2	28.6	1	C I
106	11648.0	1.3	19.3	35.9	3	C I
107	11652.8	1.6	13.5	20.7	3	C I
108	11659.7	10.4	171.8	40.2	1F	C I
109	11669.6	7.1	82.6	28.3	1	C I
110	11674.1	2.7	30.5	27.4	2	C I
111	11748.2	12.7	146.2	27.6	1	C I
112	11753.3	16.9	208.5	29.6	1	C I
113	11754.8	14.7	166.2	27.2	1	C I
114	11777.5	4.2	50.8	29.2	2	C I
115	11801.1	3.7	43.1	28.1	2	C I
116	11828.2	5.6	58.6	25.2	1	Mg I
117	11839.0	9.6	109.4	26.9	1	Ca II
118	11848.7	3.0	31.4	24.5	2	C I
119	11863.0	2.9	34.9	28.9	2	C I
120	11879.6	3.7	47.7	30.5	2	C I
121	11892.9	6.4	74.4	27.6	1	C I
122	11895.8	9.4	115.7	29.1	1	C I
123	11949.7	8.5	97.9	27.1	1	Ca II
124	11984.2	1.5	8.4	13.5	3	Si I
125	11991.6	1.8	21.4	27.2	3	Si I
126	12031.5	4.1	38.3	21.7	2	Si I
127	12074.5	1.1	20.8	46.2	3	N I
128	12083.6	4.4	54.4	28.9	2F	Mg I
129	12087.9	1.1	17.3	35.2	3	C I
130	12103.5	1.0	10.5	23.6	3	Si I
131	12135.4	3.0	42.9	32.7	2	C I
132	12168.8	1.2	12.3	23.4	3	C I
133	12186.8	0.7	6.5	22.7	3	N I
134	12192.9	1.7	28.1	37.4	3	C I
135	12244.9	0.6	14.4	55.9	3B	C I
136	12248.7	0.7	8.7	28.6	3	C I
137	12264.3	1.7	18.1	23.8	3	C I
138	12270.7	1.6	21.9	30.6	3	Si I
139	12328.8	1.1	13.8	29.3	3	N I
140	12335.6	0.9	8.3	21.4	3	C I
141	12461.3	1.8	22.3	27.7	3	N I
142	12463.8	4.3	77.9	41.3	2F	O I
143	12469.6	2.8	36.8	29.6	2	N I
144	12549.5	2.7	32.8	26.9	2	C I
145	12562.1	3.5	47.1	29.9	2B	C I
146	12569.0	2.5	62.9	⋯	2B	C I, O I
147	12581.6	3.3	50.5	34.6	2	C I
148	12590.8	0.9	15.5	38.4	3	C I
149	12601.5	3.6	50.1	31.0	2	C I
150	12614.1	6.8	98.1	32.3	1	C I
151	12818.1	⋯	⋯	⋯	1	H I (Pa β)
152	13123.4	1.3	13.0	21.2	3	Al I
153	13150.6	0.7	12.1	34.8	3	Al I
154	13163.9	9.0	179.9	42.8	1F	O I
155	13176.9	2.0	34.8	36.6	2	Si I

(This table is available in machine-readable form.)

the photon counts. The scatter is clearly small for the lines stronger than 5% in depth. Considering these trends, we classified the detected features into three strength classes: 1 for lines stronger than 5% in depth, 2 for lines with a depth of 2%–5%, and 3 for lines weaker than 2%. The lines in our line catalog are mainly ranked according to these strength classes.

The detected absorption features were then carefully identified by referring to the synthetic spectra. When multiple candidates were found for a single absorption feature, we created synthetic spectra with the candidate lines ignored one by one. If the synthetic spectrum did not change significantly, we concluded that the ignored line does not contribute to the observed feature and removed it from the candidates. When more than one line survived after this check made for every candidate, we judged the absorption feature as blended lines and added the flag "B" to the rank in our line catalog. Fine structure lines are often blended and look like an absorption feature with a single peak; thus, it is almost impossible to determine which transitions are actually detected. In such cases, we included all related transitions from VALD and MB99 regardless of $\log gf$ and added the flag "F" to the rank of the feature. Note that we did not try to measure the depth of each component for those blended or fine structure lines and assigned the same rank to them. Some of the absorption features did not have corresponding lines in the synthetic spectrum based on MB99. This is probably due to the difference in the temperatures of 21 Lyn and the Sun. In those cases, we

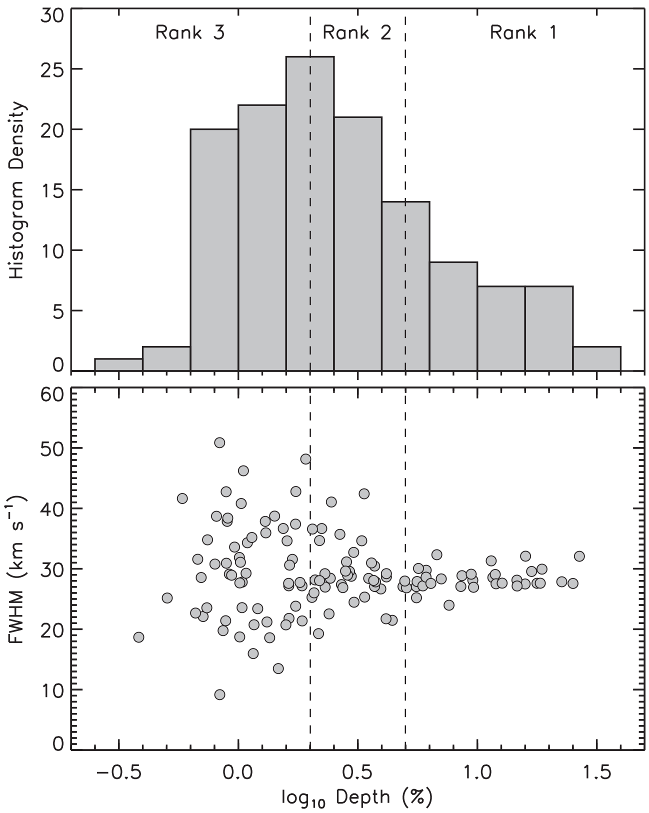

Figure 2. Histogram of the measured line depth (upper) and measured FWHM as a function of the line depth (lower). Only the unblended lines whose parameters were obtained by fitting single Gaussians are included.

only used the synthetic spectrum based on VALD for line identification.

4. Results

As a result of line identification, we conclude that the 155 absorption features are composed of 219 atomic lines including fine structure lines with minor contributions. The wavelength, the element, the log *gf* values in VALD and MB99, the excitation potential, the transition term, and the ranks of the detected lines, are summarized in the form of a line catalog in Table 4. For reference, the synthetic spectra based on this line catalog and the photospheric parameters given in Table 2 are compared with the observed spectra in Figure 1. The catalog includes the lines of H I, C I, N I, O I, Mg I, Mg II, Al I, Ca II, Fe II, and Sr II. The numbers of detected lines for individual elements are summarized in Figure 3. Figure 4 compares log *gf* and the lower excitation potential of the detected lines for each element. As was done in Gratton et al. (2006), we introduce a line-strength index $X = \log gf - \mathrm{EP} \times 5040/(0.86\, T_{\mathrm{eff}})$, where EP is the excitation potential of the lower level in electronvolts, and T_{eff} is the effective temperature in degrees Kelvin. The diagonal dashed lines in Figure 4 indicate constant X lines, and the absorption lines are expected to be strong toward the upper left corner. For comparison, the optical lines used for spectral classification or abundance analyses of A-type stars in the literature (Adelman 1994; Royer et al. 2014) are also plotted.

Besides these identified lines, the spectrum of 21 Lyn shows several features that prevented us from concluding whether the feature is a stellar line or just a spurious one for reasons such as weakness, strange line profiles, and missing synthetic spectra.

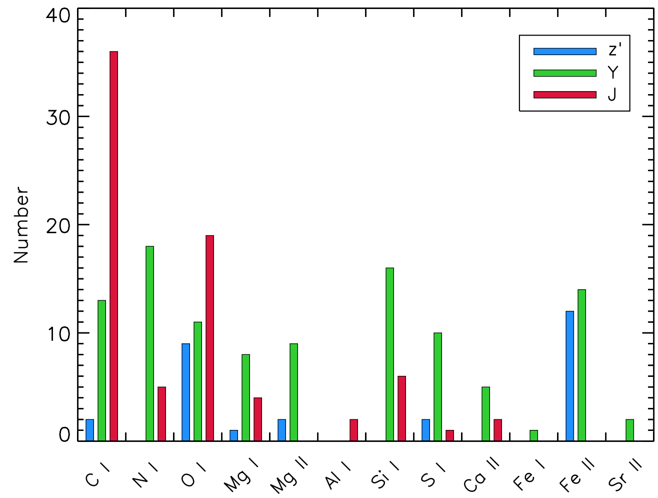

Figure 3. Number of detected lines in the observed spectra of 21 Lyn in the z', Y, and J bands.

Table 5 summarizes these unidentified features with brief notes. In the future these features need to be investigated further, hopefully with higher-quality spectra.

5. Discussion

Thanks to the high resolution and high sensitivity of WINERED, we increased the detected lines of an A-type star in the NIR drastically. In particular, the lines of various elements in the Y band (see Figure 3), a relatively unexplored band, are of scientific importance for studies of A-type stars. The richness of the detected lines suggests the possibility of spectral classification, the evaluation of chemical peculiarities, and abundance analyses of A-type stars based solely on the NIR spectra. Below, we give brief comments on how the produced line catalog would be useful for various applications.

5.1. Spectral Classification

In the optical spectrum, the strengths of the Ca II H & K lines relative to Balmer lines have been used for temperature classification (Gray & Corbally 2009). For the wavelength range of 8500–8750 Å, which is slightly shorter than our coverage, Munari & Tomasella (1999) proposed that the combination of Ca II triplet lines ($\lambda\lambda$8498, 8542, 8662) and Paschen lines serves as an indicator of the spectral type between B8 and F8 like Ca II H & K lines. As an extension of these methods, the combination of seven Ca II lines detected in this work and Paschen lines may also be used for temperature classification in the Y and J bands, which should be investigated in the future using the spectra of early-type stars with different temperatures.

5.2. Chemical Peculiarities

Preston (1974) divided chemically peculiar hot stars into four groups including Am and Ap stars. The Am stars are characterized by weak Ca II and/or Sc II lines and enhanced heavy metals. Although no Sc II line was detected in 21 Lyn, the presence of the Ca II and Fe II lines detected in this work indicates the possibility of judging whether or not a target is an Am star solely from NIR spectra. On the other hand, the characteristics of the Ap stars are strong magnetic fields and enhanced abundances of elements such as Si, Cr, Sr, and Eu.

Table 4
Line Catalog

Wavelength (Å)		Element	log *gf*		EP (eV)		Term	Rank	Notes
Air	Vacuum		VALD	MB99	lower	upper	lower − upper		
9094.8287	9097.3252	C I	+0.151	⋯	7.4878	8.8507	$^3P^o_2 - {}^3P_2$	1	ID = 1
9111.7986	9114.2997	C I	−0.297	⋯	7.4878	8.8481	$^3P^o_2 - {}^3P_1$	1	ID = 2
9122.9348	9125.4389	Fe II	+0.357	⋯	9.8492	11.2079	e $^4D_{7/2} - {}^4D^o_{7/2}$	3	ID = 3
9132.3853	9134.8919	Fe II	+0.426	⋯	9.8492	11.2065	e $^4D_{7/2} - {}^4F^o_{9/2}$	2	ID = 4
9155.8239	9158.3369	Fe II	−0.236	⋯	9.7359	11.0897	e $^6D_{5/2} - {}^6P^o_{5/2}$	3	ID = 5
9175.9196	9178.4380	Fe II	+0.479	⋯	9.9045	11.2554	e $^4D_{5/2} - {}^4F^o_{7/2}$	2	ID = 6
9178.0584	9180.5775	Fe II	+0.362	⋯	9.9408	11.2913	e $^4D_{3/2} - {}^4F^o_{5/2}$	3	ID = 7
9179.4919	9182.0113	Fe II	+0.128	⋯	9.7002	11.0505	e $^6D_{7/2} - {}^6P^o_{7/2}$	2	ID = 8
9187.1828	9189.7043	Fe II	+0.242	⋯	9.7002	11.0494	e $^6D_{7/2} - {}^6D^o_{5/2}$	2	ID = 9
9196.9217	9199.4458	Fe II	−0.002	⋯	9.9408	11.2885	e $^4D_{3/2} - {}^4D^o_{3/2}$	3	ID = 10
9204.0952	9206.6213	Fe II	+0.608	⋯	9.6536	11.0003	e $^6D_{9/2} - {}^6D^o_{9/2}$	2F	ID = 11
9204.6172	9207.1434	Fe II	+0.151	⋯	9.8492	11.1959	e $^4D_{7/2} - {}^6F^o_{7/2}$	2F	ID = 11
9212.8630	9215.3914	S I	+0.470	⋯	6.5245	7.8699	$^5S^o_2 - {}^5P_3$	1	ID = 12
9218.2500	9220.7799	Mg II	+0.270	⋯	8.6547	9.9993	$^2S_{1/2} - {}^2P^o_{3/2}$	1	ID = 13
9229.0170	9231.5498	H I (Pa ζ)	−0.735	⋯	12.0875	13.4306	$n = 3 - n = 9$	1	ID = 14
9237.5380	9240.0731	S I	+0.010	⋯	6.5245	7.8663	$^5S^o_2 - {}^5P_1$	1	ID = 15
9244.2650	9246.8019	Mg II	−0.030	⋯	8.6547	9.9955	$^2S_{1/2} - {}^2P^o_{1/2}$	1	ID = 16
9251.7872	9254.3262	Fe II	+0.125	⋯	9.7359	11.0757	e $^6D_{5/2} - {}^6D^o_{3/2}$	3	ID = 17
9255.7780	9258.3181	Mg I	−0.146	⋯	5.7532	7.0924	$^1D_2 - {}^1F^o_3$	2	ID = 18
9260.8060	9263.3474	O I	−0.241	⋯	10.7402	12.0787	$^5P_1 - {}^5D^o_0$	1F	ID = 19
9260.8480	9263.3894	O I	+0.110	⋯	10.7402	12.0787	$^5P_1 - {}^5D^o_1$	1F	ID = 19
9260.9360	9263.4775	O I	+0.002	⋯	10.7402	12.0786	$^5P_1 - {}^5D^o_2$	1F	ID = 19
9262.5820	9265.1239	O I	−0.368	⋯	10.7405	12.0787	$^5P_2 - {}^5D^o_1$	1F	ID = 20
9262.6700	9265.2119	O I	+0.224	⋯	10.7405	12.0786	$^5P_2 - {}^5D^o_2$	1F	ID = 20
9262.7760	9265.3180	O I	+0.427	⋯	10.7405	12.0786	$^5P_2 - {}^5D^o_3$	1F	ID = 20
9265.8260	9268.3688	O I	−0.718	⋯	10.7409	12.0786	$^5P_3 - {}^5D^o_2$	1F	ID = 21
9265.9320	9268.4748	O I	+0.125	⋯	10.7409	12.0786	$^5P_3 - {}^5D^o_3$	1F	ID = 21
9266.0060	9268.5488	O I	+0.712	⋯	10.7409	12.0786	$^5P_3 - {}^5D^o_4$	1F	ID = 21
9296.9197	9299.4709	Fe II	+0.018	⋯	9.9045	11.2378	e $^4D_{5/2} - {}^4D^o_{5/2}$	1	ID = 22
9603.0294	9605.6635	C I	−0.896	⋯	7.4804	8.7711	$^3P^o_0 - {}^3S_1$	1	ID = 23
9620.7822	9623.4211	C I	−0.445	⋯	7.4828	8.7711	$^3P^o_1 - {}^3S_1$	1	ID = 24
9631.8910	9634.5329	Mg II	+0.660	⋯	11.5690	12.8559	$^2D_{5/2} - {}^2F^o_{7/2}$	1F	ID = 25
9631.9470	9634.5889	Mg II	−0.640	⋯	11.5690	12.8559	$^2D_{5/2} - {}^2F^o_{5/2}$	1F	ID = 25
9632.4300	9635.0721	Mg II	+0.500	⋯	11.5691	12.8559	$^2D_{3/2} - {}^2F^o_{5/2}$	1F	ID = 25
9649.5710	9652.2177	S I	+0.250	⋯	8.4114	9.6960	$^3D^o_3 - {}^3D_3$	2	ID = 26
9658.4343	9661.0834	C I	−0.280	⋯	7.4878	8.7711	$^3P^o_2 - {}^3S_1$	1	ID = 27
9672.2840	9674.9369	S I	−0.420	⋯	8.4082	9.6897	$^3D^o_1 - {}^3D_1$	3F	ID = 28
9672.5320	9675.1849	S I	−0.970	⋯	8.4082	9.6896	$^3D^o_1 - {}^3D_2$	3F	ID = 28
9680.5610	9683.2161	S I	−1.030	⋯	8.4093	9.6897	$^3D^o_2 - {}^3D_1$	2F	ID = 29
9680.8090	9683.4642	S I	−0.010	⋯	8.4093	9.6896	$^3D^o_2 - {}^3D_2$	2F	ID = 29
9822.7500	9825.4436	N I	−0.303	⋯	11.7575	13.0194	$^4D^o_{5/2} - {}^4D_{5/2}$	3	ID = 30
9854.7588	9857.4611	Ca II	−0.205	⋯	7.5051	8.7629	$^2P^o_{1/2} - {}^2S_{1/2}$	2	ID = 31
9863.3340	9866.0386	N I	+0.080	⋯	11.7638	13.0205	$^4D^o_{7/2} - {}^4D_{7/2}$	3	ID = 32
9890.6280	9893.3400	Ca II	+0.900	⋯	8.4380	9.6912	$^2F^o_{5/2} - {}^2G_{7/2}$	1F	ID = 33
9890.6280	9893.3400	Ca II	+1.013	⋯	8.4380	9.6912	$^2F^o_{7/2} - {}^2G_{9/2}$	1F	ID = 33
9890.6280	9893.3400	Ca II	−0.531	⋯	8.4380	9.6912	$^2F^o_{7/2} - {}^2G_{7/2}$	1F	ID = 33
9909.1100	9911.8271	Fe II	+1.160	⋯	12.8225	14.0733	2[6]* − 2[7]	3B	ID = 34
9909.7016	9912.4188	S I	−0.768	⋯	8.4093	9.6600	$^3D^o_2 - {}^3P_1$	3B	ID = 34
9910.0930	9912.8103	Fe II	+1.220	⋯	12.8226	14.0733	2[6]* − 2[7]	3B	ID = 34
9931.3741	9934.0972	Ca II	+0.092	⋯	7.5148	8.7629	$^2P^o_{3/2} - {}^2S_{1/2}$	1	ID = 35
9947.0660	9949.7933	N I	−1.140	⋯	11.7575	13.0036	$^4D^o_{5/2} - {}^2F_{7/2}$	3B	ID = 36
9947.8380	9950.5655	Fe II	+1.280	⋯	12.7754	14.0214	2[7]* − 2[8]	3B	ID = 36
9997.5980	10000.339	Fe II	−1.867	⋯	5.4841	6.7239	z $^4F^o_{9/2} - {}^4G_{1/2}$	2	ID = 37
10049.373	10052.128	H I (Pa δ)	−0.303	⋯	12.0875	13.3209	$n = 3 - n = 7$	1	ID = 38
10092.095	10094.862	Mg II	+0.910	+0.96	11.6297	12.8579	$^2F^o_{5/2} - {}^2G_{7/2}$	1F	ID = 39

Table 4
(Continued)

Wavelength (Å)		Element	log *gf*		EP (eV)		Term	Rank	Notes
Air	Vacuum		VALD	MB99	lower	upper	lower – upper		
10092.217	10094.984	Mg II	+1.020	+1.07	11.6297	12.8579	$^2F^o_{7/2} - {}^2G_{9/2}$	1F	ID = 39
10092.217	10094.984	Mg II	−0.530	−0.48	11.6297	12.8579	$^2F^o_{7/2} - {}^2G_{7/2}$	1F	ID = 39
10105.132	10107.902	N I	+0.235	+0.35	11.7501	12.9767	$^4D^o_{1/2} - {}^4F_{3/2}$	2	ID = 40
10108.892	10111.663	N I	+0.443	⋯	11.7529	12.9790	$^4D^o_{3/2} - {}^4F_{5/2}$	2	ID = 41
10112.481	10115.253	N I	+0.622	+0.59	11.7575	12.9832	$^4D^o_{5/2} - {}^4F_{7/2}$	2	ID = 42
10114.640	10117.413	N I	+0.777	+0.81	11.7638	12.9893	$^4D^o_{7/2} - {}^4F_{9/2}$	1	ID = 43
10123.866	10126.642	C I	−0.031	−0.09	8.5371	9.7614	$^1P_1 - {}^1P^o_1$	1	ID = 44
10147.267	10150.049	N I	−0.169	⋯	11.7575	12.9790	$^4D^o_{5/2} - {}^4F_{5/2}$	3	ID = 45
10164.848	10167.634	N I	−0.323	⋯	11.7638	12.9832	$^4D^o_{7/2} - {}^4F_{7/2}$	3	ID = 46
10173.515	10176.303	Fe II	−2.736	−2.79	5.5107	6.7291	z $^4D^o_{7/2}$- b $^4G_{9/2}$	3	ID = 47
10216.313	10219.113	Fe I	−0.063	−0.29	4.7331	5.9464	y $^3D^o_3$ − e $^3F_4$	3	ID = 48
10245.556	10248.364	Fe II	−2.057	−1.98	6.7303	7.9401	b $^4G_{7/2}$ − y $^4G^o_{7/2}$	3	ID = 49
10327.311	10330.141	Sr II	−0.353	−0.40	1.8395	3.0397	$^2D_{5/2} - {}^2P^o_{3/2}$	2	ID = 50
10332.928	10335.760	Fe II	−1.968	⋯	6.7291	7.9286	b $^4G_{9/2}$ − y $^4G^o_{9/2}$	3	ID = 51
10366.167	10369.008	Fe II	−1.825	−1.76	6.7239	7.9197	b $^4G_{1/2}$ − y $^4G^o_{1/2}$	3	ID = 52
10371.263	10374.106	Si I	−0.705	−0.80	4.9296	6.1248	$^3P^o_1 - {}^3S_1$	3	ID = 53
10452.819	10455.684	C I	−0.722	−1.03	9.6954	10.8813	$^3F^o_2$ − 2[7/2]	3	ID = 54
10455.470	10458.335	S I	+0.250	+0.33	6.8601	8.0457	$^3S^o_1 - {}^3P_2$	1	ID = 55
10456.790	10459.656	S I	−0.447	−0.47	6.8601	8.0455	$^3S^o_1 - {}^3P_0$	2	ID = 56
10459.460	10462.326	S I	+0.030	+0.08	6.8601	8.0452	$^3S^o_1 - {}^3P_1$	1	ID = 57
10463.006	10465.874	Fe II	−2.417	−2.33	6.8031	7.9877	d $^2F_{5/2}$ − z $^2F^o_{5/2}$	3	ID = 58
10470.970	10473.840	C I	−0.672	⋯	9.6975	10.8812	$^3F^o_3$ − 2[7/2]	3	ID = 59
10501.503	10504.380	Fe II	−2.086	−2.17	5.5488	6.7291	z $^4F^o_{7/2}$ − b $^4G_{9/2}$	2	ID = 60
10507.000	10509.879	N I	+0.118	+0.23	11.8397	13.0194	$^4P^o_{3/2} - {}^4D_{5/2}$	3	ID = 61
10513.410	10516.291	N I	−0.198	−0.10	11.8374	13.0164	$^4P^o_{1/2} - {}^4D_{1/2}$	3	ID = 62
10520.580	10523.463	N I	+0.024	+0.26	11.8397	13.0179	$^4P^o_{3/2} - {}^4D_{3/2}$	3	ID = 63
10525.149	10528.034	Fe II	−2.958	−3.15	5.5526	6.7303	z $^4D^o_{5/2}$ − b $^4G_{7/2}$	3	ID = 64
10539.575	10542.463	N I	+0.530	+0.60	11.8445	13.0205	$^4P^o_{5/2} - {}^4D_{7/2}$	2	ID = 65
10541.227	10544.115	C I	−1.398	−1.27	8.5371	9.7130	$^1P_1 - {}^1P^o_1$	3	ID = 66
10546.488	10549.378	Fe II	−0.303	+0.91	9.6536	10.8289	e $^6D_{9/2}$ − y $^6F^o_{1/2}$	3	ID = 67
10549.640	10552.531	N I	+0.092	+0.15	11.8445	13.0194	$^4P^o_{5/2} - {}^4D_{5/2}$	3	ID = 68
10585.141	10588.042	Si I	+0.012	−0.06	4.9538	6.1248	$^3P^o_2 - {}^3S_1$	2	ID = 69
10603.425	10606.330	Si I	−0.305	−0.37	4.9296	6.0986	$^3P^o_1 - {}^3P_2$	2	ID = 70
10635.970	10638.884	S I	+0.460	+0.38	8.5844	9.7501	$^1D^o_2 - {}^1F_3$	2	ID = 71
10643.980	10646.896	N I	−0.639	⋯	11.8397	13.0042	$^4P^o_{3/2} - {}^4P_{1/2}$	3	ID = 72
10653.040	10655.959	N I	−0.211	⋯	11.8374	13.0009	$^4P^o_{1/2} - {}^4P_{3/2}$	3	ID = 73
10660.973	10663.893	Si I	−0.266	−0.32	4.9201	6.0827	$^3P^o_0 - {}^3P_1$	2	ID = 74
10675.668	10678.593	O I	−0.351	⋯	12.0786	13.2397	$^5D^o_4 - {}^5F_5$	3F	ID = 75
10675.668	10678.593	O I	−1.216	⋯	12.0786	13.2397	$^5D^o_4 - {}^5F_4$	3F	ID = 75
10675.668	10678.593	O I	−2.392	⋯	12.0786	13.2397	$^5D^o_4 - {}^5F_3$	3F	ID = 75
10675.766	10678.691	O I	−0.516	⋯	12.0786	13.2397	$^5D^o_3 - {}^5F_4$	3F	ID = 75
10675.766	10678.691	O I	−1.070	⋯	12.0786	13.2397	$^5D^o_3 - {}^5F_3$	3F	ID = 75
10675.766	10678.691	O I	−2.091	⋯	12.0786	13.2397	$^5D^o_3 - {}^5F_2$	3F	ID = 75
10675.906	10678.831	O I	−0.710	⋯	12.0786	13.2397	$^5D^o_2 - {}^5F_3$	3F	ID = 75
10675.906	10678.831	O I	−0.710	⋯	12.0786	13.2397	$^5D^o_2 - {}^5F_2$	3F	ID = 75
10675.906	10678.831	O I	−1.091	⋯	12.0786	13.2397	$^5D^o_2 - {}^5F_1$	3F	ID = 75
10676.023	10678.948	O I	−0.944	⋯	12.0787	13.2397	$^5D^o_1 - {}^5F_2$	3F	ID = 75
10676.023	10678.948	O I	−1.245	⋯	12.0787	13.2397	$^5D^o_1 - {}^5F_1$	3F	ID = 75
10676.079	10679.004	O I	−1.245	⋯	12.0787	13.2397	$^5D^o_0 - {}^5F_1$	3F	ID = 75
10683.080	10686.007	C I	+0.079	+0.03	7.4828	8.6430	$^3P^o_1 - {}^3D_2$	1	ID = 76
10685.340	10688.268	C I	−0.272	−0.30	7.4804	8.6404	$^3P^o_0 - {}^3D_1$	1	ID = 77
10691.245	10694.174	C I	+0.344	+0.28	7.4878	8.6472	$^3P^o_2 - {}^3D_3$	1	ID = 78
10694.251	10697.181	Si I	+0.048	+0.10	5.9639	7.1230	$^3D_2 - {}^3F^o_3$	2	ID = 79
10707.320	10710.253	C I	−0.411	−0.41	7.4828	8.6404	$^3P^o_1 - {}^3D_1$	1	ID = 80
10713.548	10716.483	N I	−0.131	⋯	11.8397	12.9967	$^4P^o_{3/2} - {}^4P_{5/2}$	3	ID = 81

Table 4
(Continued)

Wavelength (Å)		Element	log *gf*		EP (eV)		Term		Rank	Notes
Air	Vacuum		VALD	MB99	lower	upper	lower	upper		
10727.406	10730.345	Si I	+0.217	+0.29	5.9840	7.1395	$^3D_3$	$^3F^o_4$	2	ID = 82
10729.529	10732.468	C I	−0.420	−0.46	7.4878	8.6430	$^3P^o_2$	$^3D_2$	1	ID = 83
10749.378	10752.323	Si I	−0.205	−0.21	4.9296	6.0827	$^3P^o_1$	$^3P_1$	2	ID = 84
10753.980	10756.926	C I	−1.606	−1.69	7.4878	8.6404	$^3P^o_2$	$^3D_1$	2	ID = 85
10757.887	10760.834	N I	−0.389	+0.05	11.8445	12.9967	$^4P^o_{5/2}$	$^4P_{5/2}$	3	ID = 86
10786.849	10789.804	Si I	−0.303	−0.38	4.9296	6.0787	$^3P^o_1$	$^3P_0$	3	ID = 87
10811.053	10814.015	Mg I	+0.024	+0.01	5.9459	7.0924	$^3D_3$	$^3F^o_4$	2F	ID = 88
10811.084	10814.046	Mg I	−0.137	−0.16	5.9459	7.0924	$^3D_2$	$^3F^o_3$	2F	ID = 88
10811.097	10814.059	Mg I	−1.038	−0.32	5.9459	7.0924	$^3D_3$	$^3F^o_3$	2F	ID = 88
10811.122	10814.084	Mg I	−1.036	−1.05	5.9459	7.0924	$^3D_2$	$^3F^o_2$	2F	ID = 88
10811.158	10814.120	Mg I	−0.305	−1.05	5.9459	7.0924	$^3D_1$	$^3F^o_2$	2F	ID = 88
10811.198	10814.160	Mg I	−0.190	−1.93	5.9459	7.0924	$^3D_2$	$^1F^o_3$	2F	ID = 88
10811.219	10814.181	Mg I	−1.280	−1.46	5.9459	7.0924	$^3D_3$	$^1F^o_3$	2F	ID = 88
10827.088	10830.054	Si I	+0.302	+0.23	4.9538	6.0986	$^3P^o_2$	$^3P_2$	1	ID = 89
10843.858	10846.828	Si I	−0.112	−0.05	5.8625	7.0055	$^1P_1$	$^1D^o_2$	3	ID = 90
10862.652	10865.628	Fe II	−2.199	−2.11	5.5892	6.7303	z $^4F^o_{5/2}$	b $^4G_{7/2}$	2	ID = 91
10868.789	10871.767	Si I	+0.206	−0.01	6.1910	7.3314	$^3F^o_3$	2[9/2]	3	ID = 92
10869.536	10872.514	Si I	+0.371	+0.36	5.0823	6.2227	$^1P^o_1$	$^1D_2$	2	ID = 93
10885.333	10888.314	Si I	+0.221	−0.10	6.1807	7.3194	$^3F^o_2$	2[7/2]	3	ID = 94
10914.244	10917.234	Mg II	+0.020	+0.00	8.8637	9.9993	$^2D_{5/2}$	$^2P^o_{3/2}$	1B	ID = 95
10914.887	10917.877	Sr II	−0.638	−0.59	1.8047	2.9403	$^2D_{3/2}$	$^2P^o_{1/2}$	1B	ID = 95
10915.284	10918.274	Mg II	−0.930	−1.00	8.8638	9.9993	$^2D_{3/2}$	$^2P^o_{3/2}$	1B	ID = 95
10938.093	10941.089	H I (Pa γ)	+0.002	···	12.0875	13.2207	$n = 3$	$n = 6$	1	ID = 96
10951.778	10954.778	Mg II	−0.230	−0.33	8.8638	9.9955	$^2D_{3/2}$	$^2P^o_{1/2}$	1	ID = 97
10965.450	10968.454	Mg I	−0.240	−1.15	5.9328	7.0632	$^3P^o_2$	$^3D_3$	3	ID = 98
10979.308	10982.315	Si I	−0.524	−0.60	4.9538	6.0827	$^3P^o_2$	$^3P_1$	3	ID = 99
10982.058	10985.066	Si I	+0.104	−0.27	6.1910	7.3197	$^3F^o_3$	2[7/2]	3	ID = 100
11017.966	11020.984	Si I	+0.760	+0.31	6.2060	7.3310	$^3F^o_4$	2[9/2]	2	ID = 101
11125.593	11128.640	Fe II	−2.300	−2.27	5.6152	6.7293	z $^4F^o_{3/2}$	b $^4G_{5/2}$	3	ID = 102
11601.764	11604.940	S I	−0.273	−0.15	8.5844	9.6528	$^1D^o_2$	$^1P_1$	3	ID = 103
11619.282	11622.463	C I	−0.574	−0.62	8.6404	9.7072	$^3D_1$	$^3D^o_1$	2	ID = 104
11628.830	11632.014	C I	−0.260	−0.39	8.6430	9.7089	$^3D_2$	$^3D^o_2$	1	ID = 105
11647.977	11651.166	C I	−1.016	−0.83	8.6430	9.7072	$^3D_2$	$^3D^o_1$	3	ID = 106
11652.846	11656.036	C I	−0.769	−0.87	8.7711	9.8348	$^3S_1$	$^3P^o_0$	3	ID = 107
11658.820	11662.012	C I	−0.278	−0.36	8.7711	9.8343	$^3S_1$	$^3P^o_1$	1F	ID = 108
11659.680	11662.872	C I	+0.028	−0.07	8.6472	9.7102	$^3D_3$	$^3D^o_3$	1F	ID = 108
11669.626	11672.820	C I	−0.030	−0.01	8.7711	9.8333	$^3S_1$	$^3P^o_2$	1	ID = 109
11674.140	11677.336	C I	−0.795	−0.90	8.6472	9.7089	$^3D_3$	$^3D^o_2$	2	ID = 110
11748.220	11751.436	C I	+0.375	+0.40	8.6404	9.6954	$^3D_1$	$^3F^o_2$	1	ID = 111
11753.320	11756.537	C I	+0.691	+0.69	8.6472	9.7018	$^3D_3$	$^3F^o_4$	1	ID = 112
11754.760	11757.978	C I	+0.542	+0.51	8.6430	9.6975	$^3D_2$	$^3F^o_3$	1	ID = 113
11777.540	11780.764	C I	−0.520	−0.59	8.6430	9.6954	$^3D_2$	$^3F^o_2$	2	ID = 114
11801.080	11804.310	C I	−0.735	−0.80	8.6472	9.6975	$^3D_3$	$^3F^o_3$	2	ID = 115
11828.171	11831.409	Mg I	−0.333	−0.50	4.3458	5.3937	$^1P^o_1$	$^1S_0$	1	ID = 116
11838.997	11842.238	Ca II	+0.312	+0.24	6.4679	7.5148	$^2S_{1/2}$	$^2P^o_{3/2}$	1	ID = 117
11848.710	11851.953	C I	−0.697	−0.70	8.6430	9.6891	$^3D_2$	$^3P^o_2$	2	ID = 118
11862.985	11866.232	C I	−0.710	−0.70	8.6404	9.6852	$^3D_1$	$^3P^o_1$	2	ID = 119
11879.580	11882.832	C I	−0.610	−0.65	8.6404	9.6838	$^3D_1$	$^3P^o_0$	2	ID = 120
11892.898	11896.153	C I	−0.277	−0.35	8.6430	9.6852	$^3D_2$	$^3P^o_1$	1	ID = 121
11895.750	11899.006	C I	−0.008	−0.02	8.6472	9.6891	$^3D_3$	$^3P^o_2$	1	ID = 122
11949.744	11953.015	Ca II	+0.006	−0.04	6.4679	7.5051	$^2S_{1/2}$	$^2P^o_{1/2}$	1	ID = 123
11984.198	11987.478	Si I	+0.239	+0.12	4.9296	5.9639	$^3P^o_1$	$^3D_2$	3	ID = 124
11991.568	11994.850	Si I	−0.109	−0.22	4.9201	5.9537	$^3P^o_0$	$^3D_1$	3	ID = 125
12031.504	12034.796	Si I	+0.477	+0.24	4.9538	5.9840	$^3P^o_2$	$^3D_3$	2	ID = 126
12074.486	12077.791	N I	−0.082	···	12.0096	13.0362	$^2D^o_{5/2}$	$^2D_{5/2}$	3	ID = 127
12083.278	12086.585	Mg I	+0.450	−1.30	5.7532	6.7790	$^1D_2$	$^3F^o_3$	2F	ID = 128

Table 4
(Continued)

Wavelength (Å)		Element	log *gf*		EP (eV)		Term		Rank	Notes
Air	Vacuum		VALD	MB99	lower	upper	lower	upper		
12083.346	12086.653	Mg I	−0.790	−2.54	5.7532	6.7790	$^1D_2$	$^3F^o_2$	2F	ID = 128
12083.649	12086.956	Mg I	+0.410	+0.09	5.7532	6.7790	$^1D_2$	$^1F^o_3$	2F	ID = 128
12087.924	12091.232	C I	−0.525	−0.77	9.6954	10.7209	$^3F^o_2$	2[7/2]	3	ID = 129
12103.534	12106.847	Si I	−0.350	−0.49	4.9296	5.9537	$^3P^o_1$	$^3D_1$	3	ID = 130
12135.431	12138.752	C I	+0.116	⋯	9.7018	10.7231	$^3F^o_4$	2[9/2]	2	ID = 131
12168.798	12172.129	C I	−0.339	−0.40	9.6954	10.7140	$^3F^o_2$	2[7/2]	3	ID = 132
12186.840	12190.175	N I	−0.005	⋯	11.8445	12.8616	$^4P^o_{5/2}$	$^4P_{5/2}$	3	ID = 133
12192.945	12196.282	C I	−0.258	⋯	9.6975	10.7141	$^3F^o_3$	2[7/2]	3	ID = 134
12244.357	12247.708	C I	−2.008	⋯	9.7018	10.7141	$^3F^o_4$	2[7/2]	3B	ID = 135
12244.683	12248.033	C I	−1.959	⋯	9.7102	10.7225	$^3D^o_3$	2[5/2]	3B	ID = 135
12244.875	12248.225	C I	−0.784	⋯	9.7102	10.7225	$^3D^o_3$	2[5/2]	3B	ID = 135
12248.696	12252.048	C I	−0.677	−0.65	9.7089	10.7209	$^3D^o_2$	2[7/2]	3	ID = 136
12264.283	12267.639	C I	−0.272	−0.25	9.7102	10.7209	$^3D^o_3$	2[7/2]	3	ID = 137
12270.692	12274.050	Si I	−0.396	−0.54	4.9538	5.9639	$^3P^o_2$	$^3D_2$	3	ID = 138
12328.760	12332.134	N I	+0.074	⋯	11.9956	13.0009	$^4S^o_{3/2}$	$^4P_{3/2}$	3	ID = 139
12335.624	12338.999	C I	−0.532	−0.61	9.7089	10.7137	$^3D^o_2$	2[5/2]	3	ID = 140
12461.253	12464.663	N I	+0.405	⋯	12.0001	12.9948	$^2D^o_{3/2}$	$^2F_{5/2}$	3	ID = 141
12463.840	12467.250	O I	+0.104	⋯	12.0786	13.0731	$^5D^o_4$	$^5F_5$	2F	ID = 142
12463.840	12467.250	O I	−0.761	⋯	12.0786	13.0731	$^5D^o_4$	$^5F_4$	2F	ID = 142
12463.840	12467.250	O I	−1.937	⋯	12.0786	13.0731	$^5D^o_4$	$^5F_3$	2F	ID = 142
12463.974	12467.384	O I	−0.061	⋯	12.0786	13.0731	$^5D^o_3$	$^5F_4$	2F	ID = 142
12463.974	12467.384	O I	−0.614	⋯	12.0786	13.0731	$^5D^o_3$	$^5F_3$	2F	ID = 142
12463.974	12467.384	O I	−1.637	⋯	12.0786	13.0731	$^5D^o_3$	$^5F_2$	2F	ID = 142
12464.165	12467.575	O I	−0.255	⋯	12.0786	13.0731	$^5D^o_2$	$^5F_3$	2F	ID = 142
12464.165	12467.575	O I	−0.637	⋯	12.0786	13.0731	$^5D^o_2$	$^5F_2$	2F	ID = 142
12464.165	12467.575	O I	−1.636	⋯	12.0786	13.0731	$^5D^o_2$	$^5F_1$	2F	ID = 142
12464.325	12467.735	O I	−0.490	⋯	12.0787	13.0731	$^5D^o_1$	$^5F_2$	2F	ID = 142
12464.325	12467.735	O I	−0.790	⋯	12.0787	13.0731	$^5D^o_1$	$^5F_1$	2F	ID = 142
12464.401	12467.811	O I	−0.790	⋯	12.0787	13.0731	$^5D^o_0$	$^5F_1$	2F	ID = 142
12469.615	12473.027	N I	+0.610	⋯	12.0096	13.0036	$^2D^o_{5/2}$	$^2F_{7/2}$	2	ID = 143
12549.479	12552.912	C I	−0.565	−0.68	8.8466	9.8343	$^3P_0$	$^3P^o_1$	2	ID = 144
12561.993	12565.430	C I	−0.186	⋯	9.7364	10.7231	$^1F^o_3$	2[9/2]	2B	ID = 145
12562.089	12565.526	C I	−0.522	−0.65	8.8481	9.8348	$^3P_1$	$^3P^o_0$	2B	ID = 145
12569.032	12572.471	C I	−0.598	−0.72	8.8481	9.8343	$^3P_1$	$^3P^o_1$	2B	ID = 146
12569.886	12573.325	O I	−0.319	⋯	12.0870	13.0731	$^3D^o_1$	$^3F_2$	2B	ID = 146
12569.996	12573.435	O I	−0.149	⋯	12.0870	13.0731	$^3D^o_2$	$^3F_3$	2B	ID = 146
12569.996	12573.435	O I	−1.050	⋯	12.0870	13.0731	$^3D^o_2$	$^3F_2$	2B	ID = 146
12570.010	12573.449	O I	−2.560	⋯	12.0870	13.0731	$^3D^o_1$	$^3F_1$	2B	ID = 146
12570.121	12573.560	O I	−2.910	⋯	12.0870	13.0731	$^3D^o_2$	$^3F_1$	2B	ID = 146
12570.138	12573.577	O I	+0.012	⋯	12.0870	13.0731	$^3D^o_3$	$^3F_4$	2B	ID = 146
12570.138	12573.577	O I	−1.050	⋯	12.0870	13.0731	$^3D^o_3$	$^3F_3$	2B	ID = 146
12570.138	12573.577	O I	−2.600	⋯	12.0870	13.0731	$^3D^o_3$	$^3F_2$	2B	ID = 146
12581.590	12585.032	C I	−0.536	−0.67	8.8481	9.8333	$^3P_1$	$^3P^o_2$	2	ID = 147
12590.812	12594.257	C I	−0.631	⋯	9.7364	10.7209	$^1F^o_3$	2[7/2]	3	ID = 148
12601.466	12604.914	C I	−0.443	−0.58	8.8507	9.8343	$^3P_2$	$^3P^o_1$	2	ID = 149
12614.091	12617.542	C I	+0.049	−0.06	8.8507	9.8333	$^3P_2$	$^3P^o_2$	1	ID = 150
12818.077	12821.584	H I (Pa β)	+0.433	⋯	12.0875	13.0545	$n = 3$	$n = 5$	1	ID = 151
13123.410	13126.999	Al I	+0.270	+0.11	3.1427	4.0872	$^2S_{1/2}$	$^2P^o_{3/2}$	3	ID = 152
13150.753	13154.350	Al I	−0.030	−0.19	3.1427	4.0853	$^2S_{1/2}$	$^2P^o_{1/2}$	3	ID = 153
13163.889	13167.489	O I	−0.254	−0.33	10.9888	11.9304	$^3P_1$	$^3S^o_1$	1F	ID = 154
13164.858	13168.459	O I	−0.032	−0.11	10.9889	11.9304	$^3P_2$	$^3S^o_1$	1F	ID = 154
13165.131	13168.732	O I	−0.731	−0.80	10.9889	11.9304	$^3P_0$	$^3S^o_1$	1F	ID = 154
13176.888	13180.492	Si I	−0.200	−0.30	5.8625	6.8031	$^1P_1$	$^1P^o_1$	2	ID = 155

(This table is available in machine-readable form.)

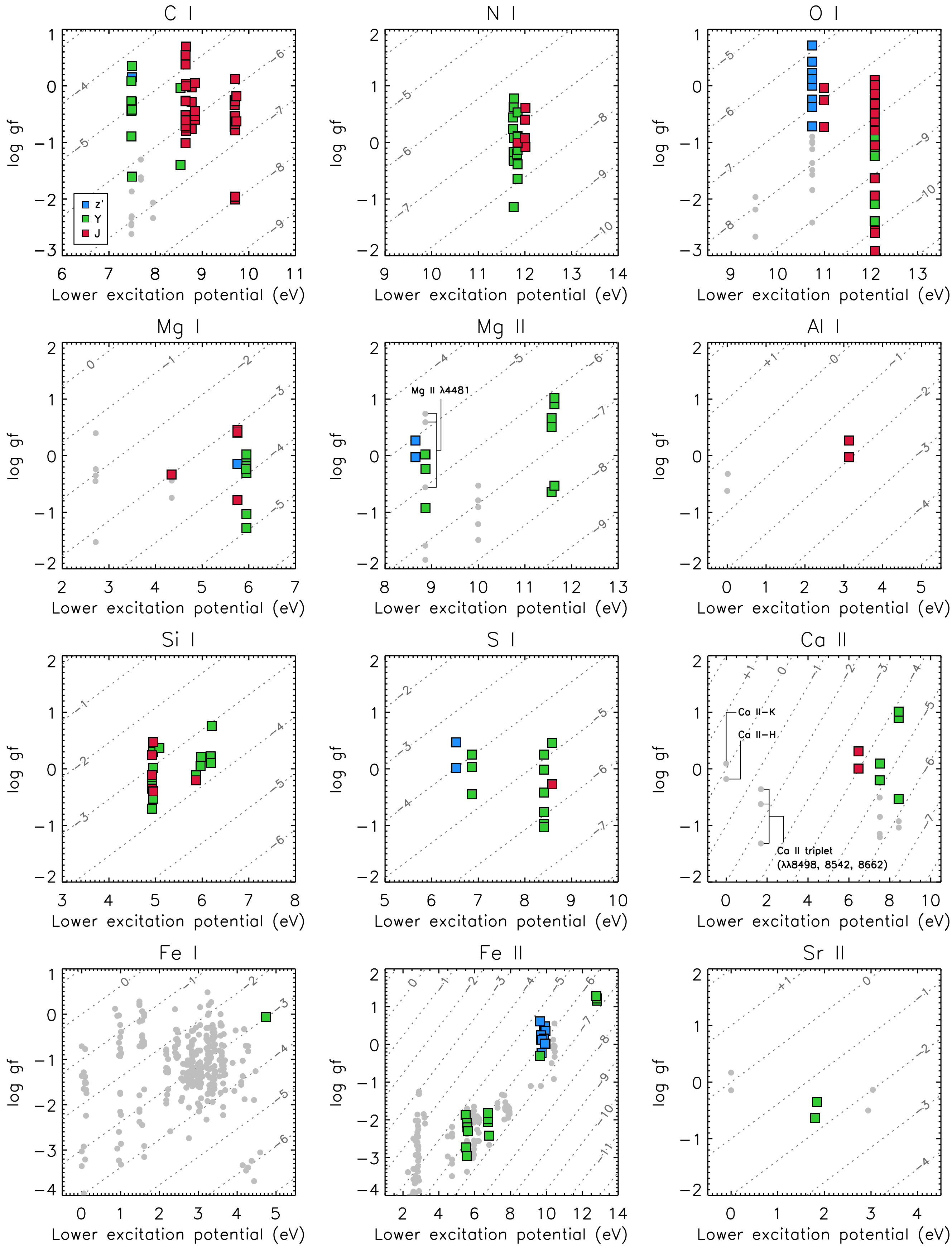

Figure 4. Distributions of the detected lines, indicated by squares (with different colors for different bands) in the log *gf*–EP plane. The diagonal dotted lines show the contours of the line-strength index *X*, and the absorption lines are expected to be strong toward the upper left corner, where *X* is larger. The absorption lines in the optical range used for spectral classification or abundance analyses in the literature are also plotted with gray circles for comparison.

Table 5
Unidentified Features in 21 Lyn

Wavelength (Å)		Notes
Air	Vacuum	
9121.1	9123.6	Possibly a stellar line Cl I λ9121.14?
9258.3	9260.8	Probably noise caused in normalization
9625.5	9628.1	Possibly a stellar line, but seriously blended with telluric absorption
9634.2	9636.8	Perhaps noise due to night-sky emission lines
9686.2	9688.9	Perhaps a stellar line. S I λ9685.87?
9701.3	9704.0	Possibly a stellar line, but blended with telluric absorption
9811.5	9814.2	Possibly a stellar line, but showing an asymmetric profile. Fe II λ9811.34?
9830.2	9832.9	Possibly a stellar line, but showing an asymmetric profile. Fe II λ9830.50?
9858.9	9861.6	Perhaps a stellar line. C I λ9859.16?
9880.0	9882.7	Likely noise because the dispersion of frames is relatively large at this part
10070.0	10072.8	Probably noise due to an instrumental defect
10434.2	10437.1	Likely a stellar line
10689.5	10692.4	Likely a stellar line. Si I λ10689.72?
10734.4	10737.3	Likely noise because the dispersion of frames is relatively large at this part
10747.2	10750.1	Likely noise
10831.4	10834.4	Likely noise due to night-sky emission lines
11611.0	11614.2	Likely noise due to heavy telluric absorption
11645.5	11648.7	Probably noise because the dispersion of frames is large at this part
11790.7	11793.9	Possibly a stellar line, but seriously blended with telluric absorption
11844.2	11847.4	Likely noise due to an instrumental defect
11866.3	11869.5	Probably noise because the dispersion of frames is large at this part
11867.8	11871.0	Probably noise because the dispersion of frames is large at this part
11901.4	11904.7	Probably noise due to an instrumental defect
12004.3	12007.6	Probably noise because the dispersion of frames is large at this part
12172.0	12175.3	Possibly a stellar line
12347.5	12350.9	Possibly a stellar line. C I λ12347.7?
12529.0	12532.4	Probably noise due to an instrumental defect
12623.2	12626.7	Probably noise because the dispersion of frames is large at this part
13241.6	13245.2	Possibly a stellar line

As can be seen in Figure 3, many Si I lines are present in the NIR. As for Sr, we detected two Sr II lines. Sr II λ10914 is heavily blended with Mg II λλ10914, 10915 and probably not a good diagnostic line for chemically peculiar stars. By contrast, the moderately strong Sr II λ10327, which is fortunately free from telluric absorption, is not blended with other lines and thus expected to be useful as a diagnostic line for Ap stars.

In addition to the Am and Ap stars, λ Bootis stars are a group of A-type stars with chemical peculiarities discovered by Morgan et al. (1943). It is known that the metal absorption lines of the λ Bootis stars are significantly weak compared to other early-type stars. In particular, Mg II λ4481 lines are important diagnostic features (Gray & Corbally 2009). Figure 5 shows a partial Grotrian diagram of the Mg II lines detected in this work and the Mg II λ4481 lines. As can be seen, Mg II λλ10914, 10915, 10951 share the lower term with Mg II λ4481 lines and are thus expected to be similarly useful for diagnostics of λ Bootis stars. Given that Mg II λλ10914, 10915 are heavily blended with Sr II λ10914, Mg II λ10951 would be a good proxy for Mg II λ4481 lines in the wavelength range of 0.90–1.35 μm.

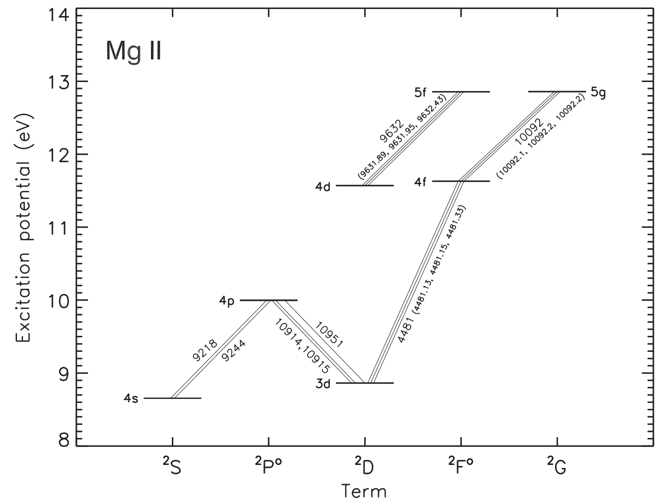

Figure 5. Partial Grotrian diagram of Mg II. The transitions of the detected lines in this work are illustrated, as well as those of Mg II λ4481 lines, which are known as diagnostic lines for λ Bootis stars.

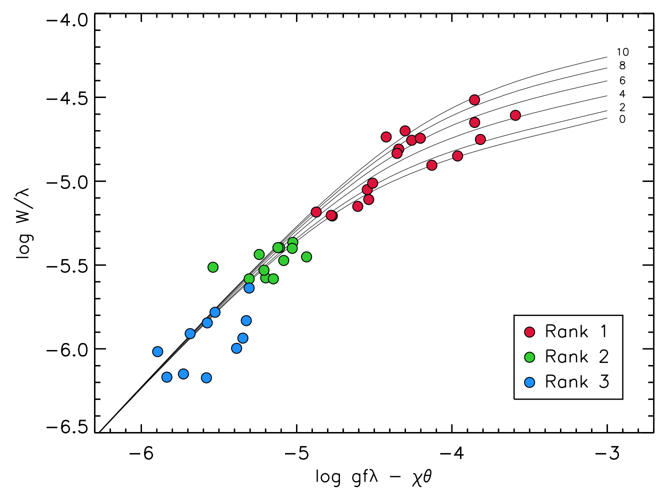

Figure 6. Empirical curve of growth for the C I lines in 21 Lyn. The symbols in the axis titles have their usual meanings (see, e.g., Gray 1992). The solid lines indicate the theoretical curves of growth created from synthetic spectra with microturbulences of $\xi = 0$, 2, 4, 6, 8, and 10 km s^{-1}. Note that the log *gf* values in the VALD database are used here.

5.3. Abundance Analysis

A large number of C I, N I, O I, Mg I, Mg II, Si I, S I, and Fe II lines in the NIR spectral range are expected to be useful for measuring CNO abundances and [α/Fe] abundance ratios solely from NIR spectra. Figure 6 shows an empirical curve of growth for the detected C I lines in 21 Lyn. Several strong lines are found in the flat part of the curve of growth and thus can be used to measure the microturbulence as well as the chemical abundance. Having many absorption lines in the NIR is important for investigating the chemical abundances of A-type stars with large interstellar extinction.

Although detailed abundance analyses are beyond the scope of this paper, the large scatter around the curve of growth seen in Figure 6 seems to be not only due to measurement errors but also due to errors in the line database. Recently, Andreasen et al. (2016) reported observationally calibrated log *gf* values for NIR Fe I lines, which were derived from the analysis of the solar spectrum. They found that the calibrated log *gf* values were different from the values in the VALD database by more than one dex for a significant number of NIR Fe I lines. These results imply the importance of observational calibration of log *gf* values for precise abundance analyses in the NIR. Establishment of line catalogs for various spectral types, which remains a challenge for our future research, would be a basis for such calibrations.

5.4. A-type Stars as Telluric Standards

As is clear in Figure 1, A-type stars are feature-rich in high-resolution spectroscopy, which should be kept in mind by observers who plan to use A-type stars as telluric standards. Our line catalog would be helpful to distinguish stellar lines from telluric absorption lines in the observed spectra of A-type stars. Sameshima et al. (2018) removed the hydrogen and metal lines from the WINERED spectra of A0 V stars to extract the telluric absorption with the help of our line catalog and accomplished high-accuracy telluric correction.

6. Summary

Aiming to extend the coverage of line catalogs in both the wavelength and spectral type directions, we are carrying out a project to establish NIR line catalogs based on observations of various types of stars using our high-dispersion echelle spectrograph, WINERED. As the first step of our project, the line catalog of an A-type star has been presented in the current paper.

The spectrum of 21 Lyn, a slowly rotating A0.5 V star, was obtained by WINERED in the wavelength range of 0.90–1.35 μm at a resolving power of $R = 28{,}000$. After the careful removal of telluric absorption using a B-type star as a telluric standard, we detected 155 absorption features, including very wide hydrogen lines in the spectrum of 21 Lyn. Line identification was then performed by visual comparison with synthetic spectra whose line information was retrieved from the VALD database and Meléndez & Barbuy (1999). The 155 absorption features were found to be composed of 219 atomic lines. Some of these lines may have only minor contributions but are included as groups of lines that reproduce ~10 features in our spectrum formed of fine structure lines.

We compiled the identified 219 atomic lines as a line catalog, in which lines are mainly ranked according to their strengths. Our line catalog includes the lines of H I, C I, N I, O I, Mg I, Mg II, Al I, Ca II, Fe II, and Sr II. In particular, the lines of various elements in the *Y* band, a relatively unexplored band, are of scientific importance for studies of A-type stars. The richness of the detected lines suggests the possibility of spectral classification, the evaluation of chemical peculiarities, and abundance analyses for A-type stars. The potential of such analyses based only on NIR spectra is important for investigating A-type stars with large interstellar extinction. Finally, our line catalog could be helpful to distinguish stellar lines from telluric absorption lines when A-type stars are used as telluric standards.

We are grateful to the staff of the Koyama Astronomical Observatory for their support during our observation. This study is financially supported by JSPS KAKENHI (grant No. 16684001, 20340042, 21840052, and 26287028) and the MEXT Supported Program for the Strategic Research Foundation at Private Universities, 2008–2012 (No. S0801061) and 2014–2018 (No. S1411028). N.M., N.K., and H.K. are supported by a JSPS Grant-in-Aid for Scientific Research (grant No. 18H01248). K.F. is supported by a JSPS Grant-in-Aid for Research Activity Start-up (grant No. 16H07323). S.H. acknowledges support from JSPS through a Grant-in-Aid for JSPS Fellows (grant No. 13J10504). N.K. is supported by JSPS-DST under the Japan-India Science Cooperative Programs during 2013–2015 and 2016–2018. This work has made use of the VALD database, operated at Uppsala University, the Institute of Astronomy RAS in Moscow, and the University of Vienna. We thank the referee, Prof. Robert Kurucz, for comments that helped us to improve this paper.

ORCID iDs

Hiroaki Sameshima https://orcid.org/0000-0001-6401-723X
Yuji Ikeda https://orcid.org/0000-0003-2380-8582
Hideyo Kawakita https://orcid.org/0000-0003-2011-9159
Natsuko Izumi https://orcid.org/0000-0003-1604-9127
Misaki Mizumoto https://orcid.org/0000-0003-2161-0361

References

Abt, H. A., & Morrell, N. I. 1995, ApJS, 99, 135
Adelman, S. J. 1994, MNRAS, 271, 355
Andreasen, D. T., Sousa, S. G., Delgado Mena, E., et al. 2016, A&A, 585, A143
Beer, A. 1852, AnP, 162, 78
Gratton, R., Bragaglia, A., Carretta, E., & Tosi, M. 2006, ApJ, 642, 462
Gray, D. F. 1992, The Observation and Analysis of Stellar Photospheres (Cambridge: Cambridge Univ. Press)
Gray, R. O., & Corbally, J. C. 2009, Stellar Spectral Classification (Princeton, NJ: Princeton Univ. Press)
Grevesse, N., & Sauval, A. J. 1998, SSRv, 85, 161
Ikeda, Y., Kobayashi, N., Kondo, S., et al. 2016, Proc. SPIE, 9908, 99085Z
Kausch, W., Noll, S., Smette, A., et al. 2015, A&A, 576, A78
Kupka, F., Piskunov, N., Ryabchikova, T. A., Stempels, H. C., & Weiss, W. W. 1999, A&AS, 138, 119
Kurucz, R. L. 1993, SYNTHE Spectrum Synthesis Programs and Line Data (Cambridge, MA: Smithsonian Astrophysical Observatory)
Livingston, W., & Wallace, L. 1991, An Atlas of the Solar Spectrum in the Infrared from 1850 to 9000 cm^{-1} (1.1 to 5.4 micrometer) (Sunspot, NM: National Solar Observatory)
Meléndez, J., & Barbuy, B. 1999, ApJS, 124, 527 (MB99)
Morgan, W. W., Keenan, P. C., & Kellman, E. 1943, An Atlas of Stellar Spectra, with an Outline of Spectral Classification (Chicago: Univ. of Chicago Press)
Munari, U., & Tomasella, L. 1999, A&AS, 137, 521
Piskunov, N. E., Kupka, F., Ryabchikova, T. A., Weiss, W. W., & Jeffery, C. S. 1995, A&AS, 112, 525
Preston, G. W. 1974, ARA&A, 12, 257
Royer, F., Gebran, M., Monier, R., et al. 2014, A&A, 562, A84
Ryabchikova, T., Piskunov, N., Kurucz, R. L., et al. 2015, PhyS, 90, 054005
Sameshima, H., Matsunaga, N., Kobayashi, N., et al. 2018, PASP, 130, 074502
Smette, A., Sana, H., Noll, S., et al. 2015, A&A, 576, A77
Wallace, L., Meyer, M. R., Hinkle, K., & Edwards, S. 2000, ApJ, 535, 325